Frequency jump using 704.4 MHz radio-frequency quadrupole and cross-bar *H*-type drift tube linear accelerators

Chuan Zhang,[1,*] Daniel Koser,[2] Nils Petry,[2] Holger Podlech,[2] and Eugene Tanke[3]

[1]*GSI Helmholtz Center for Heavy Ion Research, Planckstraße 1, D-64291 Darmstadt, Germany*
[2]*Institute for Applied Physics, Goethe University, Max-von-Laue-Straße 1, D-60438 Frankfurt a. M., Germany*
[3]*European Spallation Source ERIC, Box 176, SE-22100 Lund, Sweden*

(Received 29 October 2020; accepted 12 April 2021; published 27 April 2021; corrected 19 May 2021)

A large-scale proton or H^- accelerator often requires a jump in radio frequency, typically in the beam velocity range of $\beta = 0.4$–0.6. The MYRRHA linac has two frequency jumps: one at $\beta \cong 0.2$ and another one in the typical beam velocity range at $\beta = 0.56$. Using the MYRRHA linac as an example, this study investigates two new solutions, whereby the frequency jump in the range of $\beta = 0.4$–0.6 is eliminated. A single frequency jump at $\beta \cong 0.2$ can shorten the whole linac considerably and reduce the construction and operation costs. The proposed frequency jump sections will use 704.4 MHz radio-frequency quadrupole and cross-bar *H*-type drift tube linear accelerators. To ensure a safe and reliable cw operation at such very high frequency for these kinds of accelerating structures, careful design studies with respect to beam dynamics and rf structures including water-cooling channels have been performed. The results demonstrated the feasibility of both solutions.

DOI: 10.1103/PhysRevAccelBeams.24.040101

I. INTRODUCTION

In order to maintain high radio-frequency (rf) efficiency as well as to save construction costs, accelerating cells need to be kept reasonably short. At higher beam velocities, therefore, a large-scale proton or H^- accelerator often requires a jump in the radio frequency at which the cavities operate. Table I gives examples of existing accelerators and those under construction that use a radio-frequency jump (hereinafter abbreviated as frequency jump). It can be seen that most of them have only one frequency jump in the beam velocity range of $\beta = 0.4$–0.6, except the MYRRHA linac, which has two frequency jumps with its first frequency jump at $\beta \cong 0.2$.

The driver linac design of the MYRRHA project [5] is based on the R&D studies by a series of European accelerator-driven-system (ADS) projects. During the previous EUROTRANS project [6], the driver linac also had only one frequency jump from 352.2 to 704.4 MHz at $\beta = 0.56$. In its subsequent MAX project [7], a new frequency jump from 176.1 to 352.2 MHz was introduced at $\beta \cong 0.2$. The advantages of using a lower frequency for the injector part are (1) the feasibility of using the cost-saving four-rod radio-frequency quadrupole (RFQ) accelerator instead of the four-vane structure; (2) higher shunt impedance; (3) easier water cooling [8].

After a frequency jump, the beam-bunch length in terms of degrees is also multiplied, resulting in a reduction of the safety margin for the beam with respect to the longitudinal acceptance. Therefore, it is usually crucial to have a proper transition for minimizing the risks of beam losses at the frequency jump and in the subsequent accelerating structures.

It is well known that (1) the phase width of the beam decreases and the energy width increases during acceleration in a linac due to the phase damping effect [9]; (2) the repulsive space-charge effect decreases with the increased beam velocity [10]. For the MYRRHA linac (see Fig. 1), therefore, the second frequency jump, which happens in the range of $\beta = 0.4$–0.6 (similar to the other linacs mentioned in Table I), is less critical than the first frequency jump at $\beta \cong 0.2$ from beam dynamics point of view.

Taking the MYRRHA linac as an example, this study is focusing on new solutions for the frequency jump at $\beta \cong 0.2$. It should be mentioned that this study is not related to the MYRRHA project. In this study, the frequency jump factor of the first frequency jump for the MYRRHA linac is increased to 4. It is corresponding to a jump from 176.1 to 704.4 MHz, so that the whole driver linac will just need one frequency jump and the 352.2 MHz section between 16.6 and 172 MeV can be shortened considerably. As the MYRRHA linac is a continuous wave (cw) machine and it uses only superconducting (SC)

*c.zhang@gsi.de

TABLE I. An overview of some large-scale H^+ or H^- accelerators that use a frequency jump.

Project	Frequency before jump [MHz]	Frequency after jump [MHz]	Frequency jump factor	Transition energy [MeV]	Status
LANSCE [1]	201.25	805	4	100	In operation
SNS [2]	402.5	805	2	86.8	In operation
J-PARC [3]	324	972	3	190.8	In operation
ESS [4]	325.21	704.42	2	216	Under construction
MYRRHA	176.1	352.2	2	16.6	Under construction
[5]	352.2	704.4	2	172	

cavities after the first frequency jump, the transition has to be treated very carefully.

To accomplish the new frequency jump from 176.1 to 704.4 MHz, a section dedicated to the frequency jump will be placed directly at the end of each injector and will follow the same reliability strategy for the injector. It should have a compact layout, but the energy gain is not a design goal. The design beam current and the duty factor are still 5 mA and 100%, respectively, the same as those of the MYRRHA linac.

The design of the frequency jump section is challenging from both beam dynamics and rf cavity design points of view, because (1) almost no beam loss will be allowed according to the generally accepted beam loss limit $\leq$1 W/m for hands-on maintenance [11]; (2) an output beam with acceptable phase width and energy width as well as good beam quality should be provided to the downstream superconducting main linac; (3) last but not least, the rf parameters of the cavities have to be chosen carefully in order to ensure a very safe and reliable cw operation required by the ADS application. For the MYRRHA linac, the upper limit for beam interruptions longer than 3 seconds is only 10 per three-month operating cycle [5].

II. SOLUTION 1: USING 704.4 MHZ CH CAVITIES

Covering the energy range from 0.03 up to 16.6 MeV, the 176.1 MHz MYRRHA injector [12,13] mainly consists of one four-rod RFQ and fifteen normal-conducting (NC) cross-bar H-type (CH) drift tube linac (DTL) cavities (see Fig. 1). This study starts from a position that is 20 cm behind the last CH cavity of the injector.

Following the injector design, a natural idea is to still adopt the NC CH structure for the frequency jump section. In Fig. 2, one can see that up to now the highest frequency of the constructed NC and SC CH cavities is 360 MHz. The frequency jump CH proposed in this study has almost double that frequency, so the transverse dimensions of the structure will become much smaller. In view of a safe and reliable cw operation of such a new structure, a cavity design study with carefully chosen parameters has been performed.

At 16.6 MeV and 704.4 MHz, the cell length $\beta\lambda/2 =$ 4 cm is very similar to that of the CH-0 cavity for the GSI cw linac (now called HELIAC) [14]. The HELIAC CH-0 cavity has been built and successfully tested with beams, so its tube dimensions can be applied for the 704.4 MHz CH

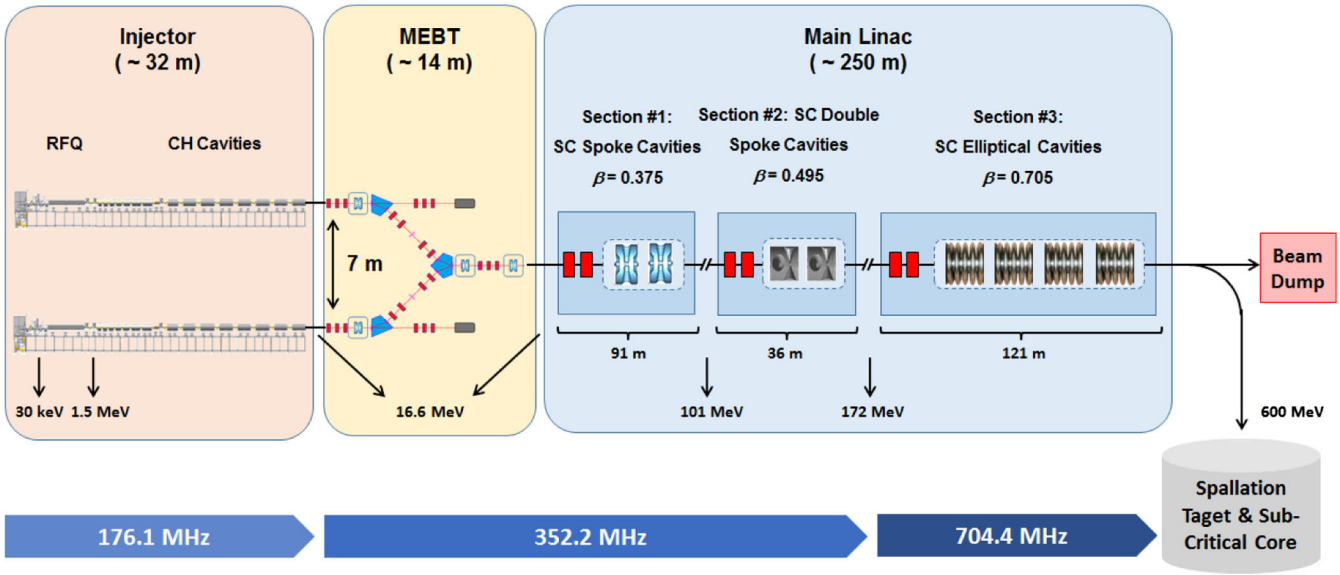

FIG. 1. Schematic layout of the MYRRHA facility.

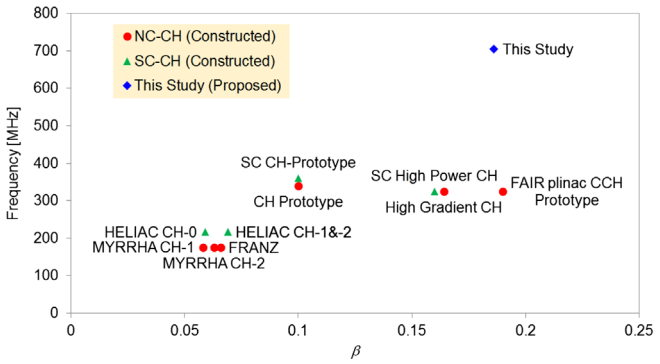

FIG. 2. Constructed CH cavities and the proposed frequency jump CH.

as well. Based on this, a seven-gap, $\beta = 0.186$, $f = 704.4$ MHz CH cavity has been designed. It is an NC cavity made of copper. Instead of looking for a high acceleration gradient, the focus of the cavity design is how to minimize rf power consumption and fulfill the requirements for working at the cw mode safely and reliably.

The main design parameters of the 704.4 MHz CH cavity as well as the simulation results given by the CST Microwave Studio (MWS) [15] are summarized in Table II. The cavity has an acceleration gradient of 0.5 MV/m and a Kilpatrick factor of 0.24, which are both very conservative for cw operation. The effective shunt impedance simulated by the MWS software is $Z_{\mathrm{eff,MWS}} = 53.46\ M\Omega/\mathrm{m}$. The CH development experience at Goethe University Frankfurt shows that the measured shunt impedance of a CH cavity is typically ~90% of the simulated value given by MWS, e.g., [16]. In this study, the rf power consumption P_c has been calculated using $Z_{\mathrm{eff,MWS}} \times 85\%$. For this 704.4 MHz CH cavity, P_c is 1.5 kW with a distribution of 60.6% on the stems, 32.2% on the drift tubes, and 7.2% on the tank wall.

Figure 3 shows the thermal simulation results using ~20 °C input cooling water for the 704.4 MHz CH structure. The adopted water-cooling concept (see Fig. 4)

TABLE II. Design parameters of a seven-gap, 704.4 MHz CH cavity.

Parameter	Value
Frequency f [MHz]	704.4
β	0.186
Gap number	7
Tank length [mm]	337
Tank inner radius [mm]	80
Tank outer radius [mm]	110
Tube inner aperture radius [mm]	10
Acceleration gradient E_{acc} [MV/m]	0.5
Shunt impedance simulated by MWS $Z_{\mathrm{eff,MWS}}$ [MΩ/m]	53.46
rf power consumption P_c [kW]	1.5 (using $Z_{\mathrm{eff,MWS}} \times 85\%$)
Kilpatrick factor	0.24

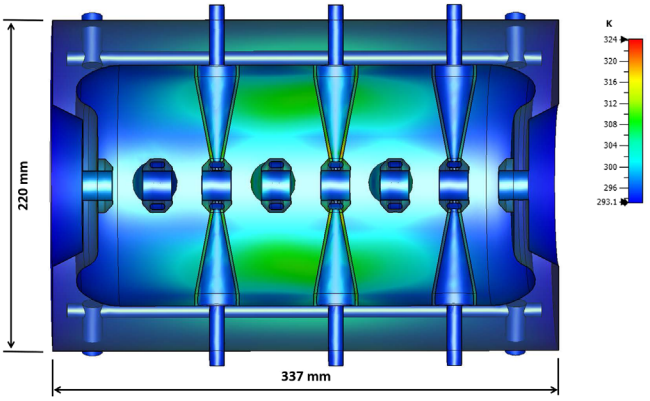

FIG. 3. Temperature distribution of the 704.4 MHz CH with 2.5 kW of input rf power and water cooling.

is as follows: (1) each pair of stems (including the tube) will be cooled by a water circuit (in darker blue); (2) the tank wall will be cooled additionally by eight water channels (in lighter blue). In order to test the robustness of the cooling design with a large safety margin, 2.5 kW of input rf power (including ~70% of additional rf power in terms of $Z_{\mathrm{eff,MWS}} \times 85\%$) was applied as a heat load to the CH cavity in the simulation.

In Fig. 3, it can be seen that even with 2.5 kW of input rf power, (1) most parts of the cavity have no obvious temperature increase; (2) the hottest spots locate on the middle stem and are close to the drift tube; (3) the highest temperature is 324 K, corresponding to a maximum temperature increase of ~30 K. According to the testing experience with the CH structures for the MYRRHA injector, this temperature distribution is safe for cw operation.

In short, all above-shown results indicate that the 704.4 MHz, $\beta \cong 0.2$ NC CH is feasible for cw operation from both mechanical and rf cavity design points of view.

As a next step, a beam dynamics design including two triplets and four 704.4 MHz CH cavities has been made for the frequency jump section. Each triplet is 36 cm long, the aperture radius of each quadrupole is 2.5 cm, and the upper limit for the quadrupole pole-tip fields is 1.2 T. Shown in Fig. 5 schematically, the whole layout is 2.71 m long, where

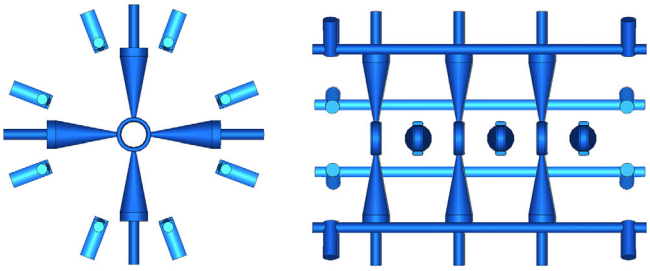

FIG. 4. Water-cooling concept for the proposed 704.4 MHz CH (left: front view; right: side view; darker blue: cooling channels for the stems and tubes; lighter blue: cooling channels for the tank wall).

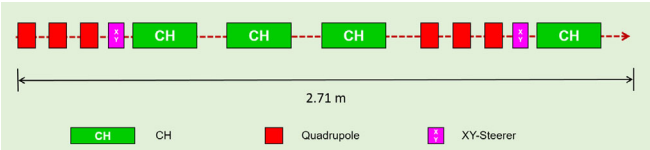

FIG. 5. Schematic layout of the frequency jump section based on four 704.4 MHz CHs.

two XY-steerer pairs (marked in magenta) have been added in front of the first and last CHs, respectively, for possible orbit corrections required by the real operation. With a design field integral up to 0.005 T m, each XY-steerer pair is 10 cm long and its aperture radius is also 2.5 cm.

Figure 6 shows that after the frequency jump the phase width (in terms of degrees) of the particles at the entrance to the first CH becomes 4 times as large as the one before the frequency jump as expected. This distribution includes 98596 macroparticles and it has been obtained using the simulated output distribution of the MYRRHA injector [12,13] as the input distribution. The phase spread of the particle distribution after the frequency jump ranges from −57° to 47°, so the frequency jump section needs to provide a proper bunching before the beam is injected into the downstream DTL cavities. Due to the 1 W/m beam loss limit, almost no particle should be lost in the frequency jump section, which is challenging for the beam dynamics design.

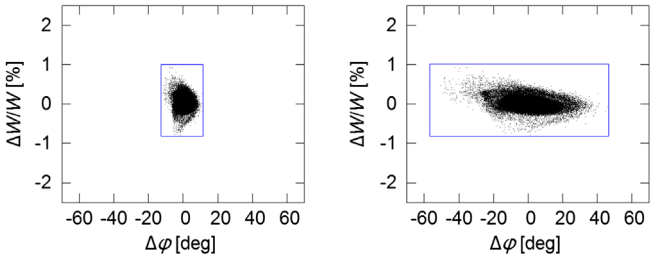

FIG. 6. Longitudinal particle distribution before (left) and after (right) frequency jump at the entrance to the first CH (the blue rectangles indicate the boundaries of the particle distributions).

For each CH, a constant synchronous phase φ_s has been used for all its gaps. The synchronous phase values for the 4 CHs are −75°, −40°, −40°, and −40°, respectively, along the beam line. The choice of $\varphi_s = -75°$ for the first CH is for the purpose of capturing all particles in the distribution after the frequency jump.

For the beam dynamics simulation, the open source DYNAC code [17] has been used. The DYNAC code originated at CERN and has undergone continuous development for several decades. The code can simulate all standard linac elements, e.g., quadrupoles, RFQ, DTL, and XY steerers. DYNAC has been benchmarked with other codes, e.g., TRACK, TRACEWIN/TOUTATIS, IMPACT and LORAS; it was also used to aid the commissioning of CERN LINAC3 and MSU (Michigan State University) ReA3; and it is being used to support the operations of ReA3 [18–24].

In the simulation, no beam loss has been found during the beam transport. The transverse emittance values are almost constant throughout the frequency jump section, and the emittance growth in the longitudinal plane is only 2.5%. Figure 7 compares the particle distribution at the entrance to the first CH (after the frequency jump) with the

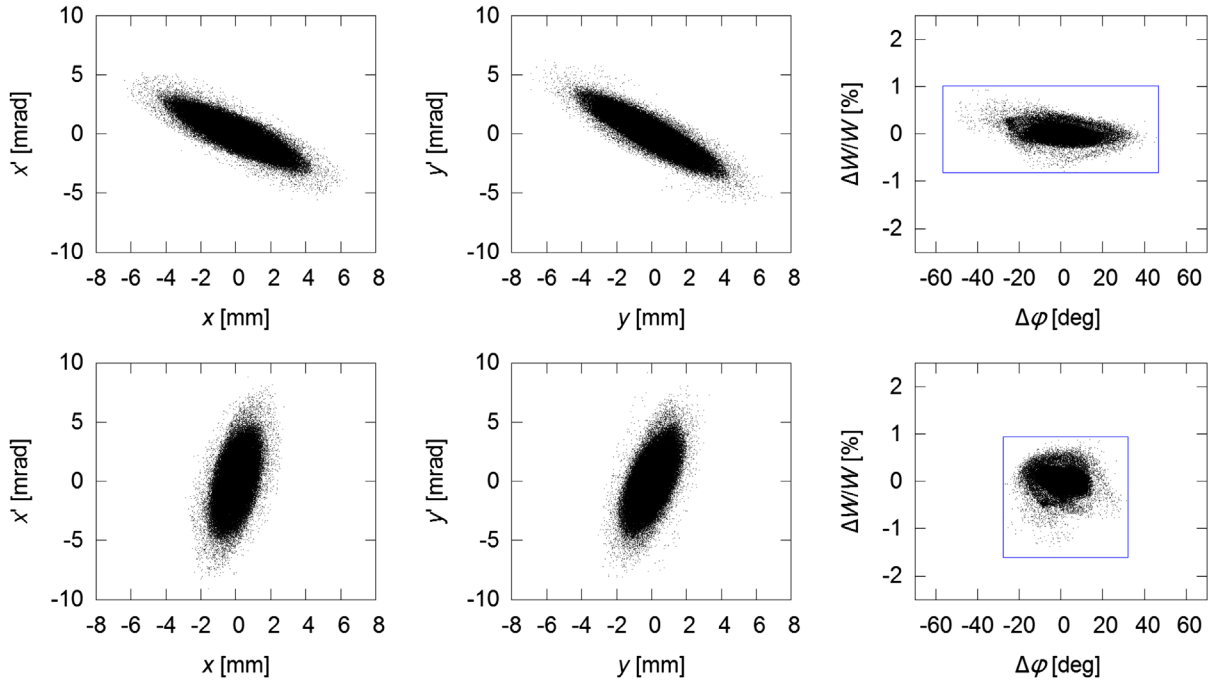

FIG. 7. Particle distribution at the entrance to the first CH after frequency jump (top) and particle distribution at the exit of the frequency jump section (bottom), where the blue rectangles indicate the boundaries of the particle distributions.

particle distribution at the exit of the frequency jump section. It can be seen that the total phase width of the beam has been decreased by more than 40° with an increase of the total energy width by only <1%. This output phase width can be well accepted by a downstream cavity operating at $\varphi_s = -40°$, which is typical for DTLs. More detailed simulation results will be presented in the next section of the paper for a comparison with another solution.

III. SOLUTION 2: USING A COMBINATION OF ONE 704.4 MHZ RFQ AND ONE 704.4 MHZ CH

In Fig. 7, one can see that the transverse beam size is roughly ±7 mm at the entrance to the first CH and ±3 mm at the exit of the frequency jump section. For the first solution (hereafter also referred to as the CH-only solution), an inner aperture radius of 10 mm has been adopted for all drift tubes. Limited by the ~4 cm cell length, it is difficult to be further enlarged. For having a larger safety margin in the beginning part of the frequency jump section, another idea is to realize this section using a four-vane RFQ accelerator. In addition, the RFQ electrodes can be more easily cooled than the small drift tubes, so this will be more favorable for cw operation.

However, different from in a CH cavity, the electric field in an RFQ has a large component in the transverse direction. To avoid a too long RFQ, the new solution will only replace the first three CHs of the first solution by an RFQ and the fourth CH is kept. One important reason for having a short RFQ is because the sensitivity to rf tuning errors for a four-vane RFQ is proportional to $(L/\lambda)^2$, where L is the RFQ length and λ is the free-space wavelength [25,26]. The CERN 750 MHz RFQ [27] which has been successfully built and tuned is ~5λ long. For an easier tuning, the length of the 704.4 MHz RFQ has been limited to be shorter than 3λ.

The evolution of the main beam dynamics design parameters along the 704.4 MHz RFQ is shown in Fig. 8, where r_0 is the midcell electrode aperture, m is the electrode modulation, B is the transverse focusing strength, U is the intervane voltage, and φ_s is the synchronous phase.

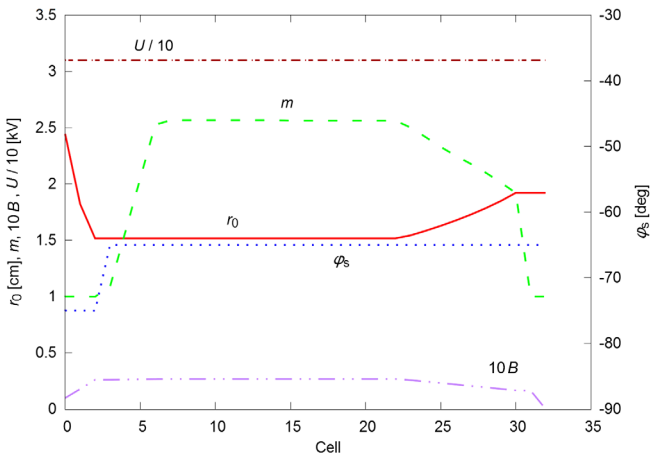

FIG. 8. Main design parameters of the 704.4 MHz RFQ.

TABLE III. Design parameters and simulation results of the 704.4 MHz RFQ.

Parameter	Value
Frequency f [MHz]	704.4
Input beam energy W_{in} [MeV]	16.6
Output beam energy W_{out} [MeV]	16.8
Intervane voltage U [kV]	31
Kilpatrick factor	0.14
Average midcell electrode aperture r_0 [cm]	1.59
Specific shunt impedance simulated by MWS $R_{p,\text{MWS}}$ [kΩ-m]	42.8
rf power consumption P_c [kW]	32.6 (using $R_{p,\text{MWS}} \times 85\%$)
RFQ length L [m]	1.23

The main design parameters as well as the rf simulation results of the 704.4 MHz RFQ are summarized in Table III. The RFQ has a total structure length of 123 cm which is equivalent to 2.9λ. The Kilpatrick factor of the 704.4 MHz RFQ is only 0.14, which is very safe for cw operation.

The RFQ shunt impedance R_p adopted by this study is defined as

$$R_p = \frac{U^2 \times L}{P_c}. \tag{1}$$

The RFQ shunt impedance simulated by MWS is $R_{p,\text{MWS}} = 42.8$ kΩ-m. The rf power consumption

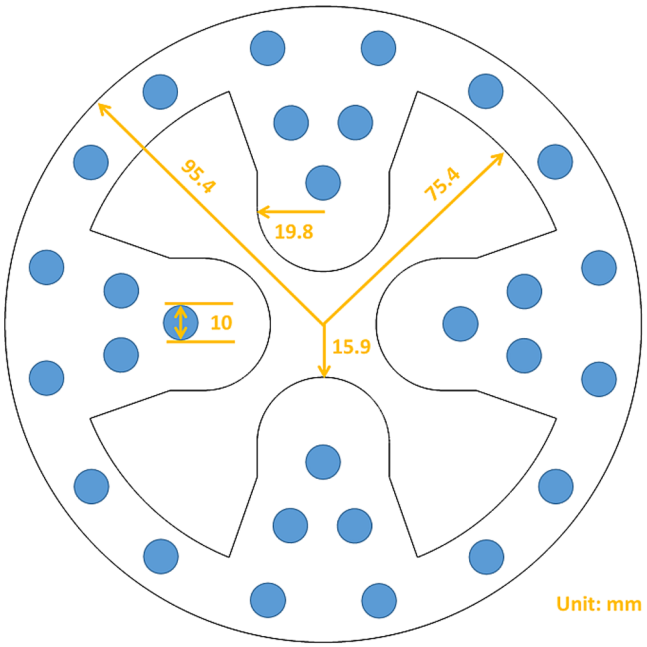

FIG. 9. Front view of the 704.4 MHz RFQ with 28 water-cooling channels (blue dots).

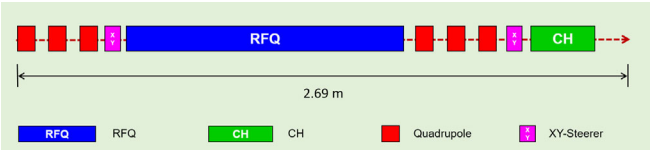

FIG. 10. Schematic layout of the frequency jump section based on a combination of one 704.4 MHz RFQ and one 704.4 MHz CH.

calculated using $R_{p,\mathrm{MWS}} \times 85\%$ is $P_c = 32.6$ kW with a distribution of 58.8% on the electrodes, 41.1% on the tank wall, and the rest on the end plates.

In Fig. 9, the transverse dimensions of the 704.4 MHz RFQ are shown. The designed 28 water-cooling channels are marked in blue. Each channel has a diameter of 10 mm.

The temperature increase ΔT as a function of the cooling-water flow rate can be calculated using Eq. (2), where ΔT is the temperature increase, P_c is the rf power consumption, $\dot{m}$ is the water flow rate per cooling channel, N_{channel} is the number of cooling channels, and C_w is the specific heat capacity of water:

$$\Delta T = \frac{P_c}{\dot{m} \times N_{\mathrm{channel}} \times C_w}. \tag{2}$$

In the test RFQ built for the MAX project, the water flow rate measured for a cooling channel which has a diameter of ~5 mm is 4.8 l/ min at a water pressure of 1 bar or 16.8 l/ min at 6 bars, the design water pressure [28,29]. According to Eq. (2), the temperature increase of the 704.4 MHz RFQ is only 3.5 K at $\dot{m} = 4.8$ l/ min or only 1 K at $\dot{m} = 16.8$ l/ min with the rf power consumption $P_c = 32.6$ kW. This is very favorable to lead to a reliable cw operation for the 704.4 MHz RFQ.

Shown in Fig. 10, the layout of solution 2 (hereafter also referred to as the RFQ-based solution) for the frequency jump section has a very similar total length as that of the CH-only solution. The same triplets and XY steerers have been adopted. Also working at $\varphi_s = -40°$, the CH used by

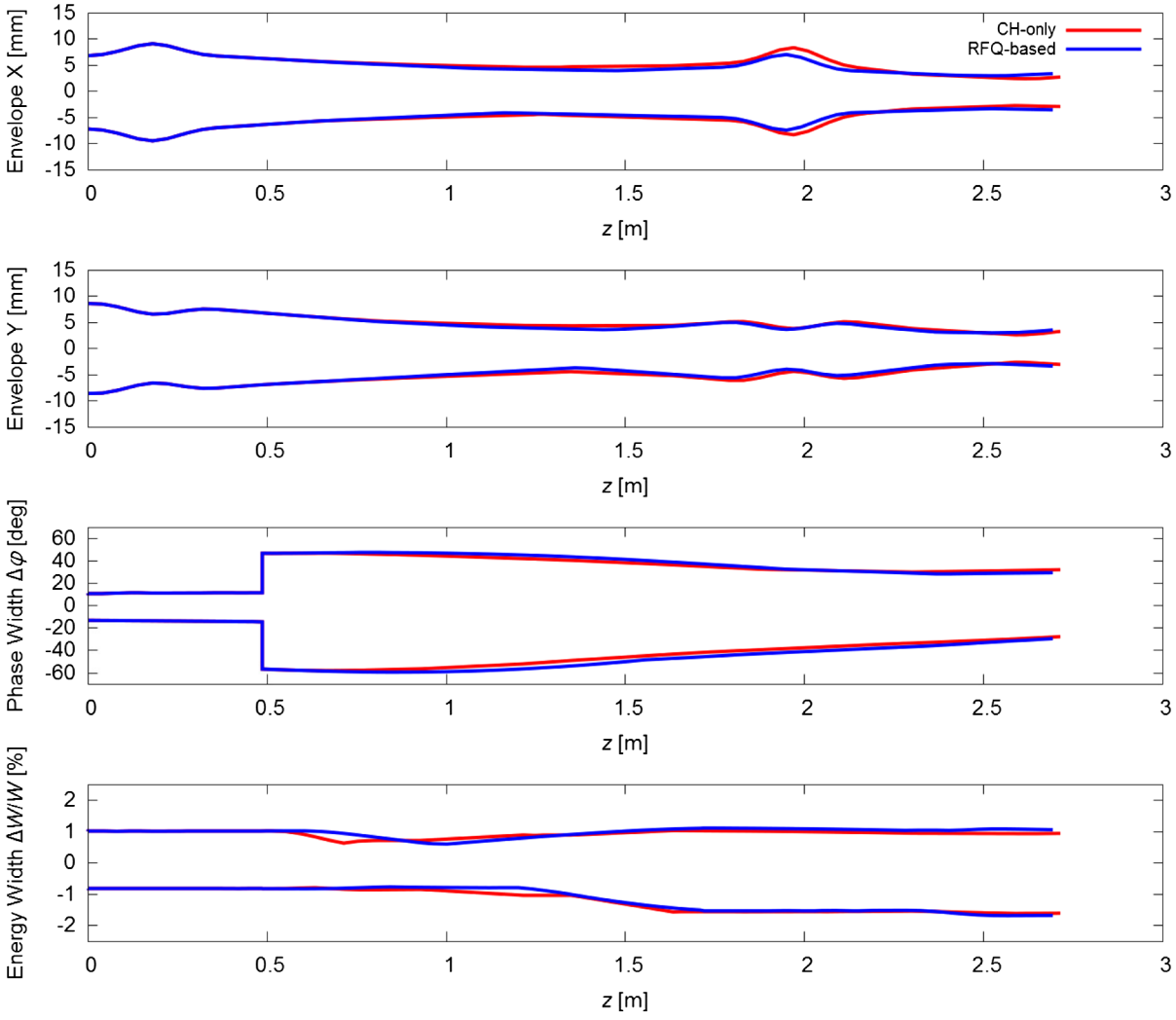

FIG. 11. A comparison of the transverse and longitudinal beam envelopes between the two solutions.

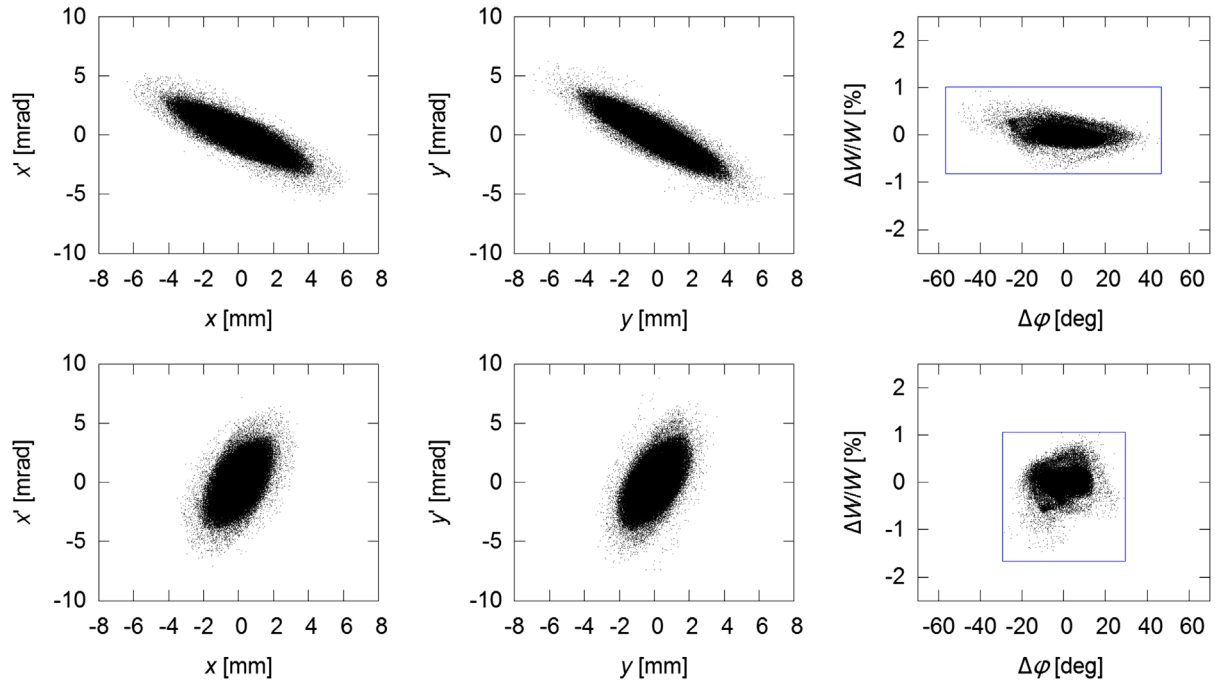

FIG. 12. Particle distribution at the entrance to the RFQ after frequency jump (top) and particle distribution at the exit of the frequency jump section (bottom), where the blue rectangles indicate the boundaries of the particle distributions.

the RFQ-based solution is almost identical to the last CH of the CH-only solution (only some small differences due to the adaption for slightly different beam energy).

The end-to-end beam dynamics simulation for the RFQ-based solution has been also performed using the DYNAC code. No beam loss has been found in the beam dynamics simulation. Figure 11 plots the transverse and longitudinal beam envelopes of both solutions, where the red and blue curves stand for the CH-only solution and the RFQ-based solution, respectively. One can see that the performance of both solutions is very similar.

Figure 12 shows the particle distributions at the entrance to the RFQ (after frequency jump) and at the exit of the frequency jump section, respectively. Generally speaking, the output distributions of the RFQ-based solution are comparable to those of the CH-only solution (see Fig. 7).

The transverse and longitudinal root-mean-square (rms) emittances as functions of position along the beam line are plotted in Fig. 13, where the solid and dashed curves stand for the CH-only solution and the RFQ-based solution, respectively. All emittance growths are very small: (1) <0.6% in the transverse planes; (2) only 2.5% and

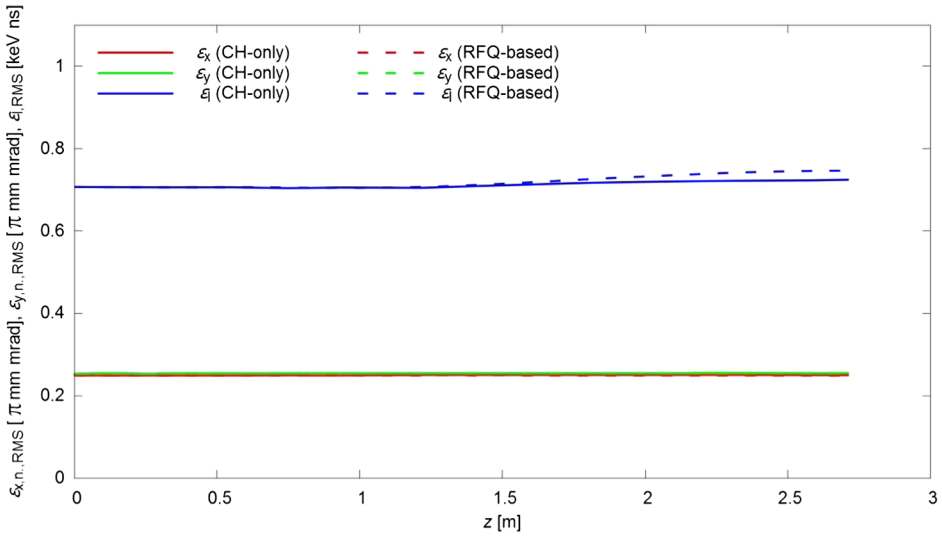

FIG. 13. A comparison of the transverse and longitudinal emittance evolutions for the two solutions.

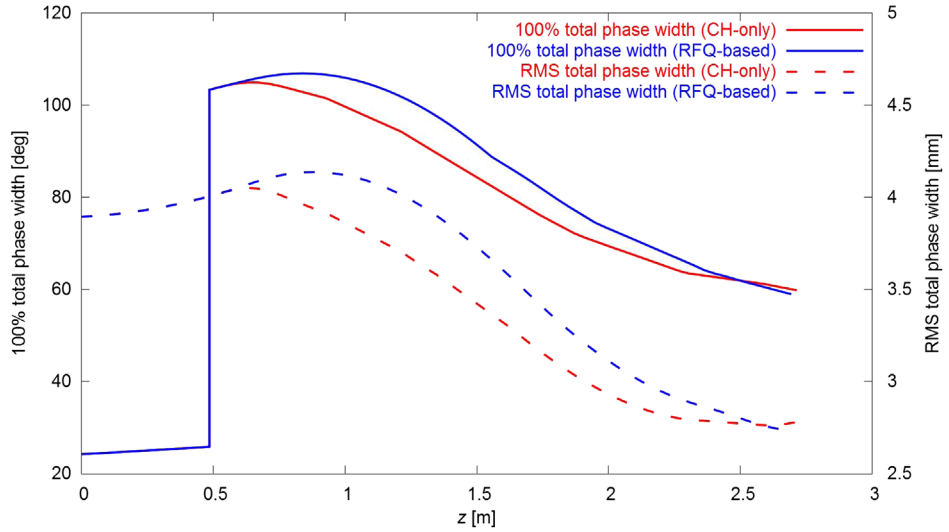

FIG. 14. A comparison of the phase width evolutions between the two solutions.

5.6% in the longitudinal plane for the CH-only solution and the RFQ-based solution, respectively.

A further comparison of the phase width evolutions between the two solutions is given in Fig. 14. From the position $z \cong 0.5$ m (location of the frequency jump) to the exit of the frequency jump section, the 100% total phase width has been reduced from ~100° to ~60° and the rms total phase width has been reduced from ~3.9 to ~2.7 mm in both cases, although the ways of bunching are different for the two solutions. In the RFQ-based case, the phase width has even an increase after the frequency jump point. This is because the bunching strength in the beginning of the RFQ-based solution is lower than that of the CH-only solution. Different than in a DTL, the electric field between the RFQ electrodes has a large transverse component, especially at the entrance where the modulation parameter is 1 for radial matching. Further downstream the longitudinal electric field strength increases, and as a consequence the bunching effect increases as well.

The main design results of the two solutions are summarized in Table IV.

TABLE IV. Comparison between the CH-only solution and the RFQ-based solution.

Parameter	CH-only	RFQ-based
Frequency f [MHz]	704.4	704.4
Cavities	4 NC CHs	1 RFQ+ 1 NC CH
Input beam energy W_{in} [MeV]	16.6	16.6
Output beam energy W_{out} [MeV]	17.0	16.9
Input emittance $\varepsilon_{x,n.,\mathrm{RMS}}$ [π mm mrad]	0.249	0.249
Input emittance $\varepsilon_{y,n.,\mathrm{RMS}}$ [π mm mrad]	0.254	0.254
Input emittance $\varepsilon_{l,\mathrm{RMS}}$ [keV ns]	0.707	0.707
Emittance growth $\Delta\varepsilon_x$ [%]	0.51	0.06
Emittance growth $\Delta\varepsilon_y$ [%]	0.52	0.21
Emittance growth $\Delta\varepsilon_l$ [%]	2.48	5.57
Total layout length L_{layout} [m]	2.71	2.69

IV. ERROR STUDIES

Based on the three settings defined in Table V, systematic error studies have been carried out for both solutions. The following different kinds of errors have been included: (1) transverse offsets of the input beam with respect to (with respect to) the ideal beam axis (IBOF); (2) roll-pitch-yaw rotations of the input beam with respect to the ideal beam axis (IBRO); (3) transverse offsets of the magnetic lenses with respect to the ideal beam axis (LOFF); (4) roll-pitch-yaw rotations of the magnetic lenses with respect to the ideal beam axis (LROT); (5) transverse offsets of the tanks with respect to the ideal beam axis (TOFF); (6) roll-pitch-yaw rotations of the tanks with respect to the ideal beam axis (TROT); (7) voltage amplitude errors for the tanks (VERR); and (8) phase errors for the tanks (PERR). For each solution, three batches of error studies have been

TABLE V. Settings of the ranges for generating random errors.

Error type	Error range setting for batch 1	Error range setting for batch 2	Error range setting for batch 3
IBOF [mm]	±0.2	±0.3	±0.4
IBRO [mrad]	±2.0	±3.0	±4.0
LOFF [mm]	±0.2	±0.3	±0.4
LROT [mrad]	±2.0	±3.0	±4.0
TOFF [mm]	±0.2	±0.3	±0.4
TROT [mrad]	±2.0	±3.0	±4.0
VERR [%]	±2.0	±3.0	±4.0
PERR [°]	±2.0	±3.0	±4.0

TABLE VI. An overview of the beam transmission efficiency values for the six batches[a].

	S1B1	S1B2	S1B3	S2B1	S2B2	S2B3
T_{max} [%]	100	100	100	100	100	100
T_{min} [%]	95.25	10.67	0	100	98.46	34.07
$N_{runs,T\geq 99\%}$ [%]	99.9	89.82	69.93	100	99.9	96.25
$N_{runs,90\%\leq T<99\%}$ [%]	0.1	6.15	12.01	0	0.1	2.69
$N_{runs,T<90\%}$ [%]	0	4.03	18.06	0	0	1.06

[a]S1B1 means "solution 1 (CH only), batch 1," S2B2 means "solution 2 (RFQ based), batch 2," and so on for the other batch codes.

performed. Every batch includes 1040 runs with randomly generated and mixed errors. From batch 1 to batch 3, the error ranges are gradually enlarged. For an easy description of the six batches, each batch is named by a four-character code, e.g., S1B1 which means "solution 1 (CH-only), batch 1" and S2B2 which means "solution 2 (RFQ-based), batch 2."

The statistics results of the beam transmission efficiency, T, for the six batches are summarized in Table VI. In the table, T_{max} and T_{min} are the highest and lowest transmission for each batch, respectively, while $N_{runs,T\geq 99\%}$, $N_{runs,90\%\leq T<99\%}$, and $N_{runs,T<90\%}$ are the ratio of the runs in a batch with T higher than 99%, between 90% and 99%,

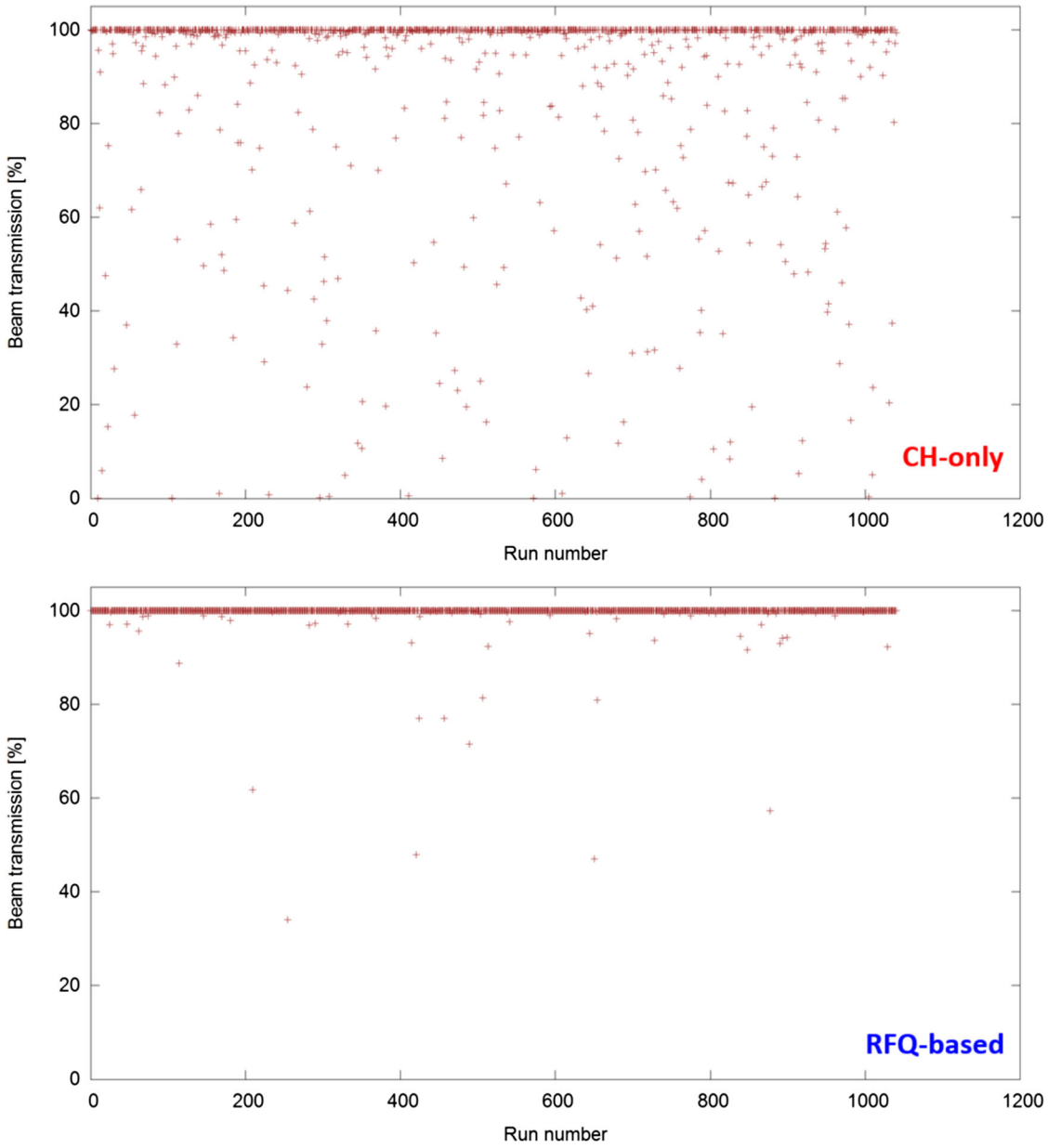

FIG. 15. Beam transmission efficiency as a function of the run number for batch 3 of the CH-only solution (top) and batch 3 of the RFQ-based solution (bottom), respectively.

TABLE VII. An overview of the additional emittance growths for the six batches[a].

	S1B1	S1B2	S1B3	S2B1	S2B2	S2B3
$\delta\varepsilon_{x,\max}$ [%]	0.54	0.72	0.93	0.02	0.03	2.83
$\delta\varepsilon_{x,\min}$ [%]	−5.11	−52.40	−71.63	−0.18	−4.04	−53.98
$\delta\varepsilon_{y,\max}$ [%]	0.62	2.99	3.32	0.03	0.26	4.43
$\delta\varepsilon_{y,\min}$ [%]	−0.96	−44.29	−72.80	−0.07	−0.48	−34.60
$\delta\varepsilon_{z,\max}$ [%]	1.17	1.98	62.48	0.82	2.42	5.32
$\delta\varepsilon_{z,\min}$ [%]	−0.41	−6.56	−8.99	−0.42	−0.62	−5.60
$N_{\text{runs},\lvert\delta\varepsilon x\rvert>1\%}$ [%]	0.19	9.32	27.19	0	0.38	4.52
$N_{\text{runs},\lvert\delta\varepsilon y\rvert>1\%}$ [%]	0	6.69	25.46	0	0	3.26
$N_{\text{runs},\lvert\delta\varepsilon z\rvert>1\%}$ [%]	1.06	11.04	28.43	0	2.02	9.90

[a]S1B1 means "solution 1 (CH only), batch 1," S2B2 means "solution 2 (RFQ based), batch 2," and so on for the other batch codes.

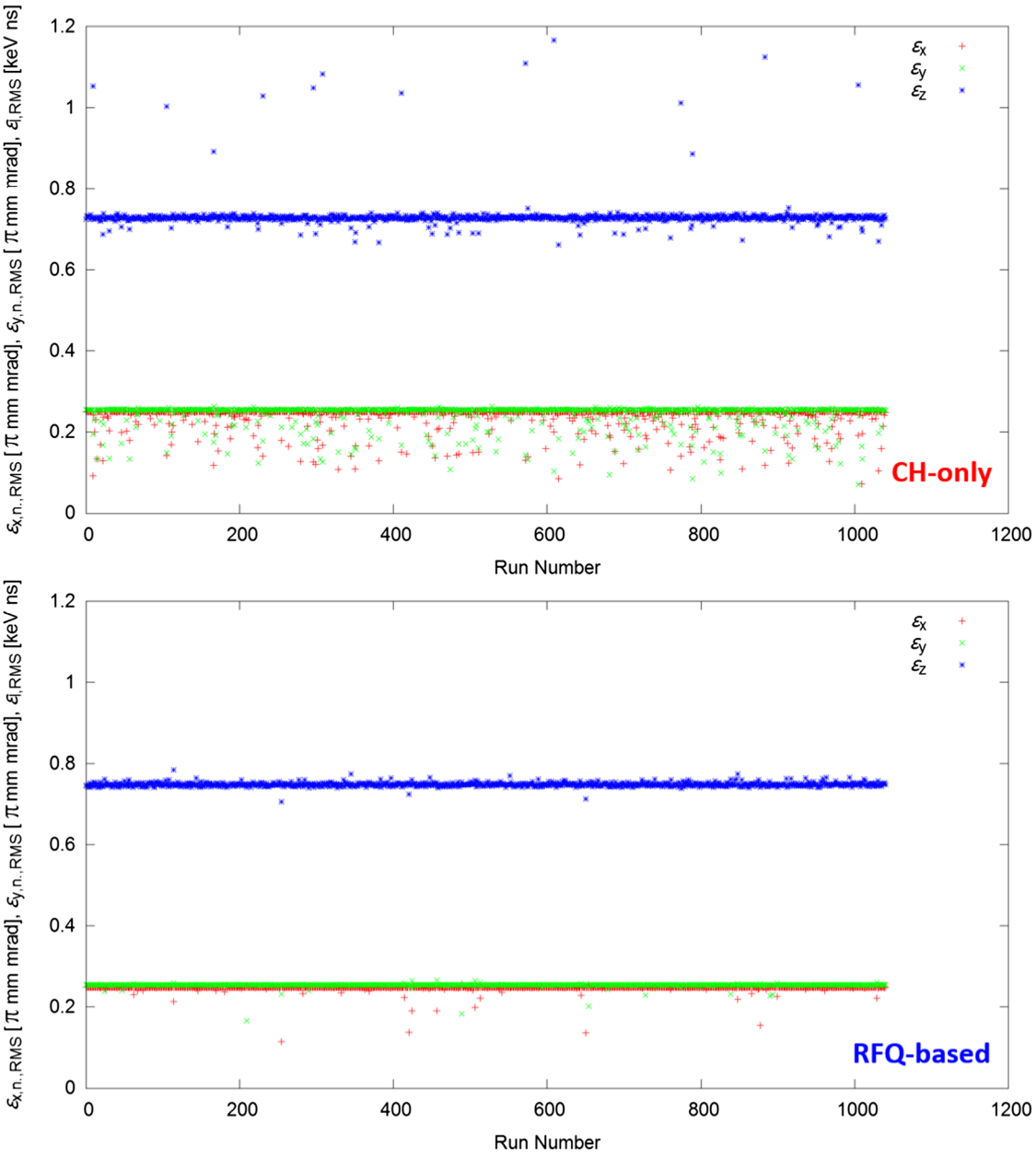

FIG. 16. Output emittances as a function of the run number for batch 3 of the CH-only solution (top) and batch 3 of the RFQ-based solution (bottom), respectively.

and lower than 90% respectively. It can be seen that the RFQ-based solution shows better robustness against errors than the CH-only solution. With the batch-1 setting, 0.1% of the CH-only runs have <5% beam losses and all RFQ-based runs have 100% of beam transmission. With the batch-2 setting, the CH-only solution starts to have runs with obvious beam losses, while only 0.1% of the RFQ-based runs have <2% beam losses. With the batch-3 setting, two of the 1040 CH-only runs lost all particles, but 96.25% of the RFQ-based runs still have $T \geq 99\%$.

The beam transmission efficiency values of the batch-3 runs for both solutions are visualized in Fig. 15. So far, no orbit correction has been applied. For the CH-only solution, >30% of runs have >1% beam losses and the lowest transmission is 0%, while for the RFQ-based solution, <4% of runs have >1% beam losses and the lowest transmission is >34%. It can be seen again that the RFQ-based solution has a much larger tolerance to the errors than the CH-only solution.

Also the so-called additional emittance growth $\delta\varepsilon$, defined in Eq. (3), has been compared for the six batches:

$$\delta\varepsilon = \frac{\varepsilon_{\text{out}}^{\text{with errors}} - \varepsilon_{\text{out}}^{\text{without errors}}}{\varepsilon_{\text{in}}}. \tag{3}$$

For each batch, the maximum and minimum $\delta\varepsilon$ in all three planes are listed in Table VII. Except a few batch-3 runs of the CH-only solution have large positive additional emittance growths in the longitudinal plane, the $\delta\varepsilon$ values for all other runs are small or negative. The large $|\delta\varepsilon_{\text{min}}|$ values in the transverse planes for some batches are due to beam losses. Furthermore, the ratio of the runs with $|\delta\varepsilon| > 1\%$ are also calculated for all batches and listed in the table. It can be seen that the $\delta\varepsilon$ values of most runs for the RFQ-based solution are within the range of $\pm 1\%$.

Figure 16 plots the output emittances of all batch-3 runs as a function of the run number for both solutions. It again clearly shows that with the batch-3 setting the RFQ-based

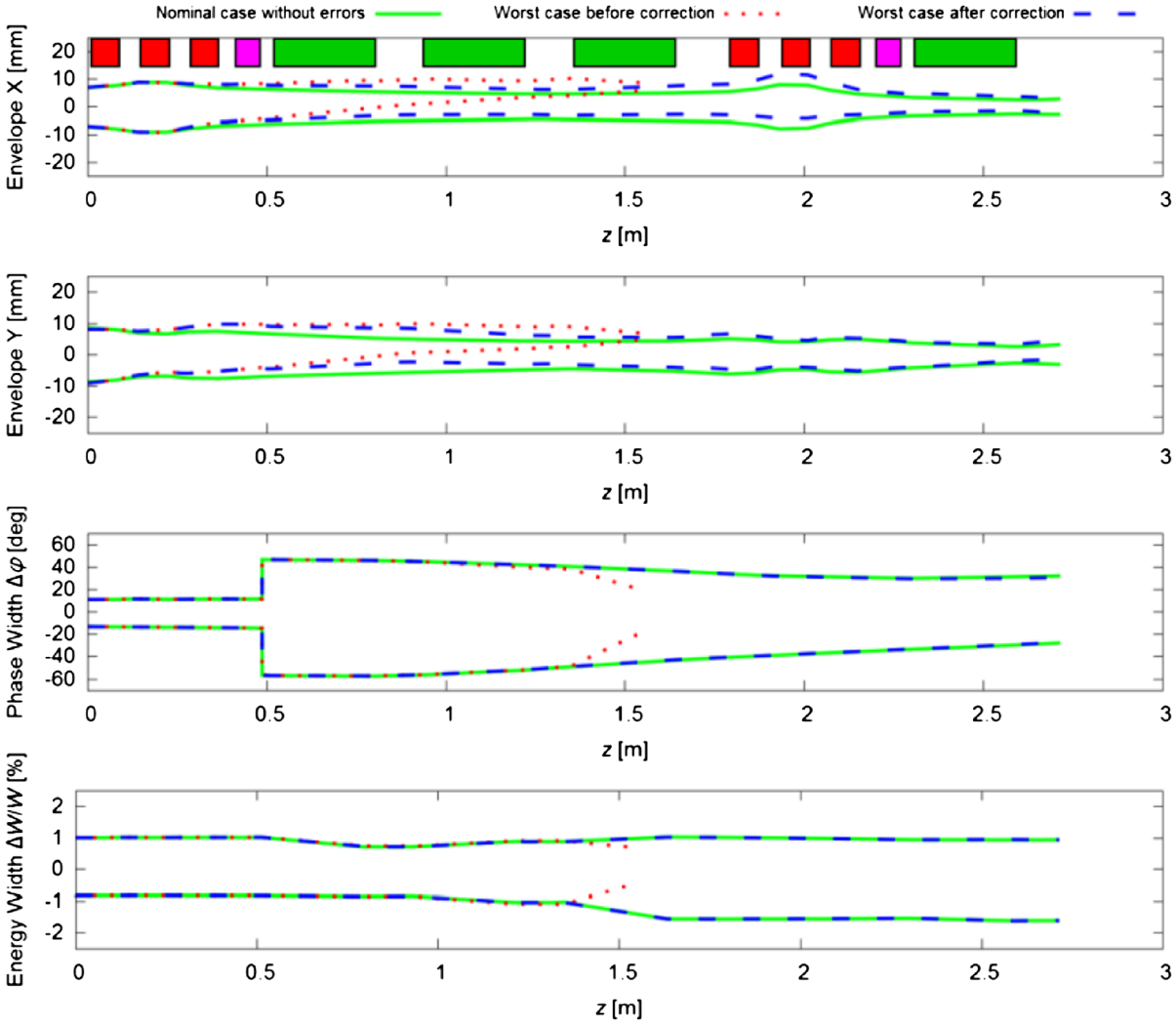

FIG. 17. Transverse and longitudinal beam envelopes of the worst run in S1B3 (green: nominal case without errors; red: worst case before correction; blue: worst case after correction).

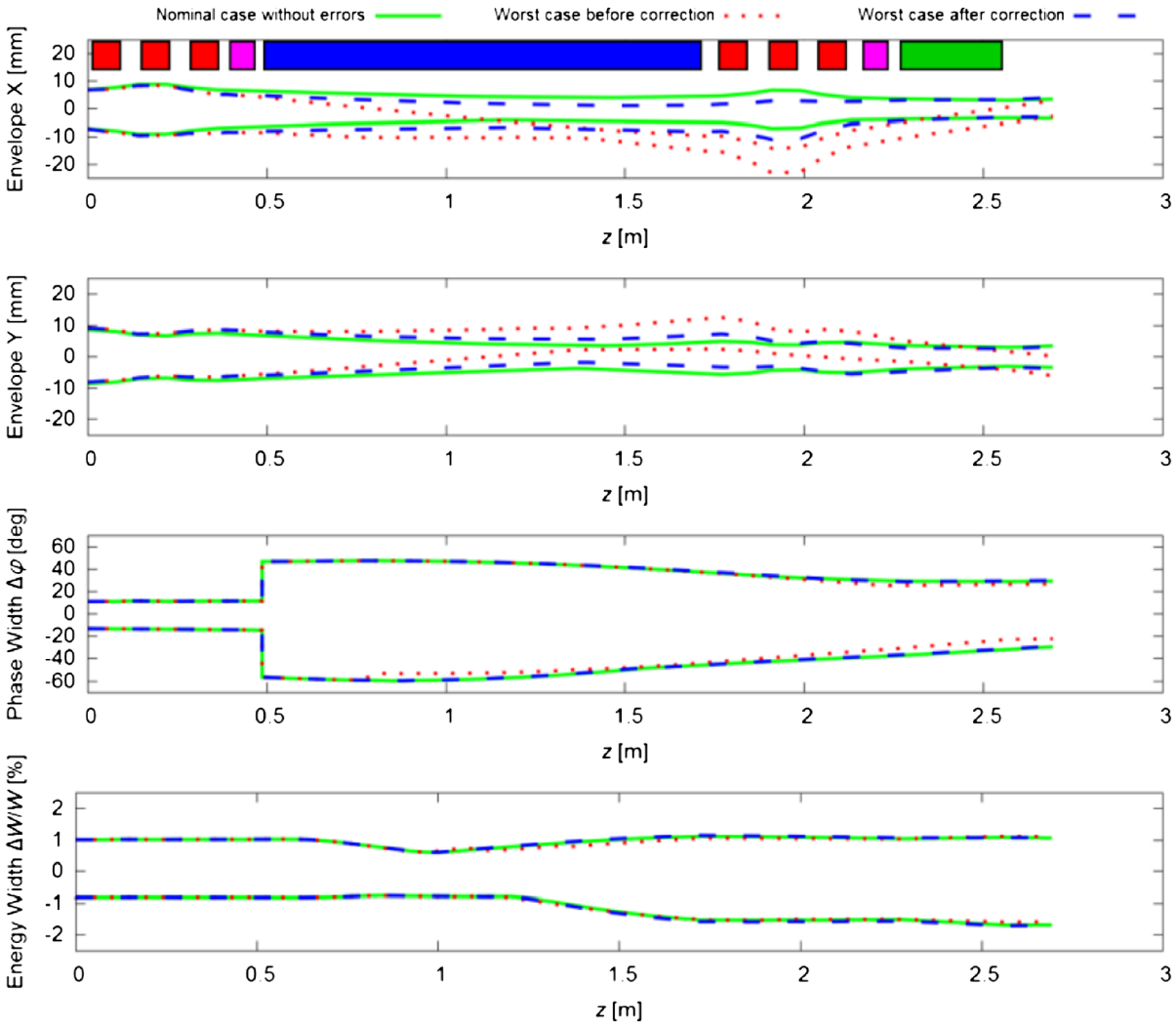

FIG. 18. Transverse and longitudinal beam envelopes of the worst run in S2B3 (green: nominal case without errors; red: worst case before correction; blue: worst case after correction).

solution is much less sensitive to the errors than the CH-only solution. The obviously decreased output emittances have been caused by beam losses.

For both solutions, one XY-steerer pair after each of the two triplets has been foreseen (see Figs. 5 and 10). The design field integral for the steerers is up to 0.005 T m. Based on these steerers, orbit corrections have been performed for the worst cases of the S1B3 and S2B3 batches. Here the worst case is defined as the run with the lowest beam transmission. When the number of runs with the lowest transmission in a batch is more than 1, the run which reaches this transmission at the earliest will be taken as the worst case.

Figures 17 and 18 show the transverse and longitudinal beam envelopes before and after the orbit correction for the worst runs of S1B3 and S2B3, respectively. For a better comparison, the design envelopes (without errors) have also been shown. For both worst runs, the beam losses happened in the transverse planes (for the worst run of S1B3: losses mainly located in the CH1, CH2 and CH3 cavities; for the worst run of S2B3: losses mainly located in the RFQ).

The correction results are as follows: (1) the beam losses for both cases have disappeared; (2) the corrected longitudinal envelopes almost overlap with the nominal ones; (3) at the output, the corrected transverse beam sizes are very close to the nominal ones; (4) the new additional emittance growths are $\delta\varepsilon_x = -0.21\%$, $\delta\varepsilon_y = 0.32\%$, $\delta\varepsilon_z = 0.43\%$ and $\delta\varepsilon_x = -0.05\%$, $\delta\varepsilon_y = 0.01\%$, $\delta\varepsilon_z = 0.33\%$ for the two runs, respectively.

V. CONCLUSIONS

Two new solutions for a frequency jump at $\beta \cong 0.2$ have been introduced. The first solution is mainly based on four 704.4 MHz NC CH cavities, while the second one is mainly using a combination of one 704.4 MHz RFQ and one 704.4 MHz NC CH.

The frequency jump sections provided by the two solutions are both only ∼2.7 m long. It is worth adding such a short section, as it allows the replacement of a potentially long lower frequency section (∼140 m long at 352.2 MHz in the MYRRHA example) with a more compact higher frequency section (at 704.4 MHz in the MYRRHA example). For the same β, the cell length at 704.4 MHz is half the one at 352.2 MHz, so a 704.4 MHz cavity will have double the number of cells per cavity than a 352.2 MHz one if they have the same length. The current MYRRHA main linac has two 352.2 MHz sections [5]: (1) one uses the SC single (two cells) Spoke cavities with a design $E_{\mathrm{acc}} = 7$ MV/m; (2) the other uses the SC double (three cells) Spoke cavities with a design $E_{\mathrm{acc}} = 6.8$ MV/m.

In case 704.4 MHz Spoke cavities with four or six cells are not available, the SC CH structure [30] can be a potential candidate to replace the two groups of 352.2 MHz Spoke cavities. For this, four-cell and six-cell 704.4 MHz SC CH cavities could be used. The SC CH structure was originally developed as a kind of efficient multicell SC structure [30]. A seven-cell SC CH cavity has been built and successfully tested with beams [14]. For this study, an MWS simulation of a seven-cell, $\beta = 0.2$, SC CH cavity shows that this kind of structure also works at 704.4 MHz. Lowering the E_{acc} values from 7 and 6.8 MV/m to 5.5–6 MV/m for a larger safety margin, a calculation has been performed for the acceleration using the four-cell and six-cell 704.4 MHz SC CH cavities between the frequency jump section and the elliptical-cavity section. To reach the end energy values of the two original 352.2 MHz sections, 101 and 172 MeV, the required numbers of four-cell and six-cell SC CH cavities are 46 and 14, respectively. For both sections, the number of required cavities is reduced by ∼25% (in the original design, 60 and 18 cavities were adopted, respectively [5]). Accordingly, less magnets and beam diagnostic elements will be needed. This shows the efficiency of the proposed frequency jump solutions.

The two frequency jump solutions have very similar beam performance at their nominal settings, e.g., in terms of beam transmission, beam envelopes, and the evolution of the emittances. Both longitudinal output distributions have a half phase width of ∼30° and a half energy width of 1.3%, which are also within the longitudinal acceptance of the current MYRRHA main linac [5] if the small energy difference is ignored.

The performed error studies have shown that (1) by means of two XY-steerer pairs, one can avoid all losses for the worst cases of both solutions via the orbit correction; (2) the correction can restore the beam sizes as well as the emittances of the output beam close to those of the nominal cases; (3) the RFQ-based solution is more robust in the presence of errors than the CH-only solution.

At 704.4 MHz, the cavities used by the two solutions have relatively small transverse dimensions. In view of reliable cw operation, different water-cooling concepts have been developed. The thermal calculation has shown that (1) the temperature increases of the RFQ and CH cavities will be low enough for a reliable cw operation; (2) at 704.4 MHz, the RFQ electrodes can be more easily cooled than the small CH drift tubes.

In short, both solutions for the frequency jump are feasible, but the RFQ-based solution can provide larger safety margins for both beam transport and heat load. Although the RFQ-based solution will be more expensive in construction and operation, it is worthy to adopt the RFQ-based solution, because (1) the RFQ-based solution can provide a safer and more reliable operation than the CH-only solution, which is very important for the ADS application; (2) the increased costs in construction and operation will be partially and possibly completely mitigated, as the frequency jump solution will shorten the whole linac considerably.

For this study, these two frequency jump solutions were developed taking reliable cw operation as a high priority. For pulsed machines, higher electrode voltages will be feasible, so the beam bunching with the two solutions could be performed even more efficiently. Especially for the RFQ-based solution, if the bunching provided by the RFQ with higher electrode voltages is sufficient, one can have a pure RFQ solution for the frequency jump. For example, spallation neutron source applications with a duty factor of several percent can be promising candidates for the proposed frequency jump solutions.

As the next steps, prototypes for the proposed 704.4 MHz NC cavities are planned to be built and tested. Because CERN has successfully built two 750 MHz RFQs [27], we will first focus on the R&D of the novel 704.4 MHz NC CH. For the construction of such a relatively small cavity, the 3D printing technology is a choice under consideration. In addition, the 704.4 MHz SC CH will also be further studied as a candidate structure to cover the acceleration between the frequency jump section and the elliptical-cavity section.

ACKNOWLEDGMENTS

Many thanks go to C. Mühle, K. Kümpel, and F. Bouly for the valuable discussions on steering magnets, water cooling in CH cavities, and the longitudinal acceptance of the MYRRHA main linac, respectively.

[1] R. W. Garnett, LANSCE accelerator update and future plans, *J. Phys. Conf. Ser.* 1021, 012001 (2018).

[2] N. Holtkamp, Status of the SNS linac: An overview, in *Proceedings of LINAC 2004* (JACOW, Lübeck, Germany, 2004), p. 837.

[3] Y. Liu, T. Maruta, T. Miyao, M. Otani, K. Futatsukawa, A. Miura, and S. Fukuoka, Progresses of J-PARC linac commissioning, in *Proceedings of the 14th Annual Meeting*

of the Particle Accelerator Society of Japan (Sapporo, Japan, 2017), p. 885.

[4] I. D. Kittelmann, F. S. Alves, E. Bergman, C. Derrez, V. Grishin, T. Grandsaert, T. J. Shea, W. Cichalewski, G. W. Jabłoński, W. Jałmużna, and R. Kiełbik, Ionization chamber based beam loss monitoring system for the ESS linac, in *Proceedings of IBIC2019* (JACoW, Malmö, Sweden, 2019), p. 136.

[5] F. Bouly, M. Baylac, A. Gatera, and D. Uriot, Superconducting linac design upgrade in view of the 100 MeV MYRRHA phase I, in *Proceedings of IPAC2019* (JACoW, Melbourne, Australia, 2019), p. 837.

[6] H. Podlech, S. Barbanotti, A. Bechtold, J.-L. Biarrotte, M. Busch, S. Bousson, F. Dziuba, R. Gobin, T. Junquera, H. Klein, M. Luong, A. C. Mueller, G. Olry, N. Panzeri, P. Pierini, U. Ratzinger, R. Tiede, and C. Zhang, The EUROTRANS project, *AIP Conf. Proc. No.* 1265 (AIP, New York, 2010), p. 355; https://doi.org/10.1063/1.3480201.

[7] http://ipnwww.in2p3.fr/MAX/.

[8] C. Zhang, H. Klein, D. Mäder, H. Podlech, U. Ratzinger, A. Schempp, and R. Tiede, From EUROTRANS to MAX: New strategies and approaches for the injector development, in *Proceedings of IPAC2011* (JACoW, San Sebastián, Spain, 2011), p. 2583.

[9] T. P. Wangler, *RF Linear Accelerators* (Wiley-VCH Verlag GmbH & Co., KG, Berlin, 2008).

[10] K. Schindl, Space charge, in *Proceedings of CAS–CERN Accelerator School: Intermediate Course on Accelerator Physics, Zeuthen, Germany* (CERN, Geneva, 2003), p. 305.

[11] F. Gerigk, K. Bongardt, and I. Hofmann, High current linac design with examples of resonances and halo, in *Proceedings of LINAC2002* (JACoW, Gyeongju, Korea, 2002), p. 569.

[12] D. Mäder *et al.*, Status and development of the MYRRHA injector, in *Proceedings of IPAC2018* (JACoW, Vancouver, BC, Canada, 2018), p. 432.

[13] K. Kümpel, S. Lamprecht, P Müller, N. F. Petry, H. Podlech, and S. Zimmermann, Status of the MYRRHA CH cavities, in *Proceedings of IPAC2018* (JACoW, Vancouver, BC, Canada, 2018), p. 193.

[14] W. Barth, K. Aulenbacher, M. Basten, M. Busch, F. Dziuba, V. Gettmann, M. Heilmann, T. Kürzeder, M. Miski-Oglu, H. Podlech, A. Rubin, A. Schnase, M. Schwarz, and S. Yaramyshev, First heavy ion beam tests with a superconducting multigap CH cavity, Phys. Rev. Accel. Beams **21**, 020102 (2018).

[15] CST Microwave Studio (new name: CST Studio Suite), https://www.3ds.com/products-services/simulia/products/cst-studio-suite/.

[16] N. F. Petry, S. Huneck, K. Kümpel, H. Podlech, U. Ratzinger, and M. Schwarz, Test of a high power room temperature CH DTL cavity, in *Proceedings of IPAC2017* (JACoW, Copenhagen, Denmark, 2017), p. 2237.

[17] http://dynac.web.cern.ch/dynac/dynac.html.

[18] J.-H. Jang, I. S. Hong, H. Jang, D. Jeon, H. Jinpresenter, and H. J. Kim, Beam optics of RISP linac using DYNAC code, in *Proceedings of IPAC2015* (JACoW, Richmond, VA, 2015), p. 3845.

[19] E. Tanke, M. Eshraqi, R. Miyamoto, A. Ponton, R. de Prisco, E. Sargsyan, and S. Valero, Benchmark of beam dynamics code DYNAC using the ESS proton linac, in *Proceedings of LINAC2014* (JACoW, Geneva, Switzerland, 2014), p. 945.

[20] E. Tanke, M. Eshraqi, Y. Levinsen, A. Ponton, and S. Valero, Status of and plans for the beam dynamics program DYNAC, in *Proceedings of LINAC2016* (JACoW, East Lansing, MI, 2016), p. 80.

[21] T. Yoshimoto and M. Ikegami, IMPACT model for ReA and its benchmark with DYNAC, in *Proceedings of LINAC2016* (JACoW, East Lansing, MI, 2016), p. 601.

[22] P. Lapostolle, E. Tanke, and S. Valero, Comparison of computational methods and results concerning the simulation of IH structures with the codes LORAS and DYNAC, Report No. PS/Hi/Note 92-02, CERN, 1992.

[23] Y. Bylinsky, H. Kugler, P. Lapostolle, U. Ratzinger, E. Tanke, S. Valero, and D. Warner, Dynamics and tolerances for the CERN interdigital H linac, in *Proceedings of LINAC1992* (JACoW, Ottawa, Ontario, Canada, 1992), p. 220.

[24] W. Wittmer, D. Alt, S. Krause, D. Leitner, S. Nash, R. Rencsok, J. A. Rodriguez, M. Syphers, and X. Wu, Online modeling of the rare isotope reaccelerator—ReA3, in *Proceedings of IPAC2014* (JACoW, Dresden, Germany, 2014), p. 3195.

[25] L. M. Young, Tuning and stabilization of RFQ's, in *Proceedings of LINAC1990* (JACoW, Albuquerque, New Mexico, 1990), p. 530.

[26] D. D. Armstrong, W. D. Cornelius, F. O. Purser, R. A. Jameson, and T. P. Wangler, RFQ development at Los Alamos, Report No. LA-UR-84-498, Los Alamos National Laboratory, 1984.

[27] M. Vretenar, V. A. Dimov, M. Garlasché, A. Grudiev, B. Koubek, A. M. Lombardi, S. Mathot, D. Mazur, E. Montesinos, and M. Timmins, High-frequency compact RFQs for medical and industrial applications, in *Proceedings of LINAC2016* (JACoW, East Lansing, MI, 2016), p. 704.

[28] H. Podlech, P. Müller, C. Lenz, A. Schempp, M. Vossberg, and C. Zhang, Design of the MYRRHA RFQ and associated short test section, Deliverable No. 2.4, MAX project (EUROTAM Contract No. 269565), 2014.

[29] M. Vossberg, C. Lenz, H. Podlech, A. Schempp, and A. Bechtold, RF measurement during cw operation of an RFQ prototype, in *Proceedings of IPAC2013* (JACoW, Shanghai, China, 2013), p. 2720.

[30] H. Podlech, U. Ratzinger, H. Klein, C. Commenda, H. Liebermann, and A. Sauer, Superconducting CH structure, Phys. Rev. ST Accel. Beams **10**, 080101 (2007).

Correction: Equation (1) contained a minor error and has been fixed.